PROCEEDINGS OF SCIENCE

# Double Higgs production at CMS

**Florian Bury**[a,*] **on behalf of the CMS collaboration**

[a] *Université catholique de Louvain,*
*Pl. de l'Université 1, 1348 Ottignies-Louvain-la-Neuve, Belgium*

*E-mail:* florian.bury@cern.ch

The double Higgs production is the only direct probe of the Higgs self-coupling interaction, and could prove to be a valuable source of information about the scalar potential. Due to destructive interference, the cross-section of this process is heavily suppressed and remains a challenging measurement. This document presents the different non-resonant analyses, public as of July 2022, performed by the CMS collaboration using the 138 $fb^{-1}$ data of Run-2 in the various decay channels, as well as their combination. Results are interpreted in terms of cross-sections and couplings, notably the trilinear Higgs interaction.

*41st International Conference on High Energy physics - ICHEP2022*
*6-13 July, 2022*
*Bologna, Italy*

*Speaker





PoS(ICHEP2022)507

## 1. Motivations

The Higgs scalar potential is usually parameterized as

$$V(\phi^\dagger\phi) = -\mu^2(\phi^\dagger\phi) + \lambda(\phi^\dagger\phi)^2, \tag{1}$$

where the vacuum expectation value (VEV) $v$ corresponds to the minimum of the potential, such that $\mu^2 = \lambda v$. After electroweak symmetry breaking (EWSB) the potential gives rise, among other things, to a scalar particle identified as the Higgs boson with a Lagrangian of the form

$$\mathcal{L}_{scalar} \ni \frac{1}{2}\left(\partial_\mu h \partial^\mu h\right) - \lambda v^2 h^2 - \lambda v h^3 - \frac{\lambda}{4}h^4 - \frac{\lambda v^4}{4}. \tag{2}$$

In eq. (2), the first term corresponds to the kinetic term of this scalar particle, the second is a mass term that was measured in 2012 with the Higgs discovery [1, 2], the third corresponds to a triple Higgs interaction vertex and the fourth to a quartic interaction. The latter is expected to be too suppressed for it to be measured in the foreseeable future, but the trilinear interaction is of particular interest. The value of the VEV obtained from the W and Z mass measurements and from the Higgs mass allow to predict $\lambda$ assuming the standard model (SM) and therefore the trilinear coupling value. Measuring this coupling would not only provide a test of the SM, but also gives some insight about the true shape of the scalar potential.

The only way to probe the trilinear coupling directly at leading order is through the double Higgs (HH) production. The main productions modes are gluon-gluon fusion (GGF) and vector-boson fusion (VBF). The leading diagrams associated to these modes are on fig. 1, and their cross-sections are respectively of 31.05 fb $\pm 3\%(\text{PDF}+\alpha_S)\,^{+2.2\%}_{-5\%}$ (scale) $\pm 2.6\%(m_t)$ and 1.73 fb $\pm 2.1\%(\text{PDF}+\alpha_S)\,^{+0.03\%}_{-0.04\%}$ (scale) at 13 TeV [3]. Unfortunately, due to destructive interference between the different diagrams, the cross-section is about a thousand times smaller than for single Higgs production. This makes HH measurements already challenging. One upside is that there is a strong dependence of the cross-section on the trilinear coupling (fig. 2), which helps setting constraints on this parameter.

In the $\kappa$-framework the different couplings to the Higgs boson are modified by a factor $\kappa$ (coupling modifier), for example for the trilinear interaction $\kappa_\lambda \equiv \lambda/\lambda_{SM}$. Similarly, the coupling between vector bosons and a pair of Higgs boson only present in VBF is modified by $\kappa_{2V}$, together with $\kappa_\lambda$ they can only be accessed directly through HH production.

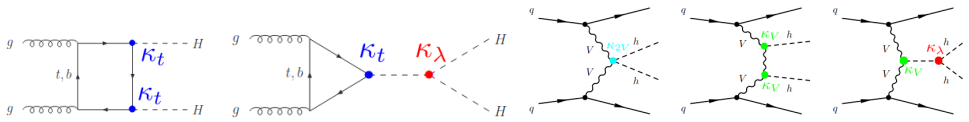


**Figure 1:** Main HH GGF (left) and VBF (right) diagrams. From Ref. [3].

Another challenge in HH searches resides in the numerous decay channels (2, right), each of them coming with its own branching ratio (BR) value and challenges. For example, the bbbb decay channel has the largest BR it also suffers from a QCD multi-jet contamination, while the bb$\gamma\gamma$ has one of the smallest BR but has an outstanding signal discrimination due to the precise diphoton invariant mass measurement. Without a golden channel, as many channels as possible must be included to provide the most sensitive measurements. In this document all public CMS [4]

HH results as of July 2022 using the complete Run-2 dataset are presented as well as their latest combination results.

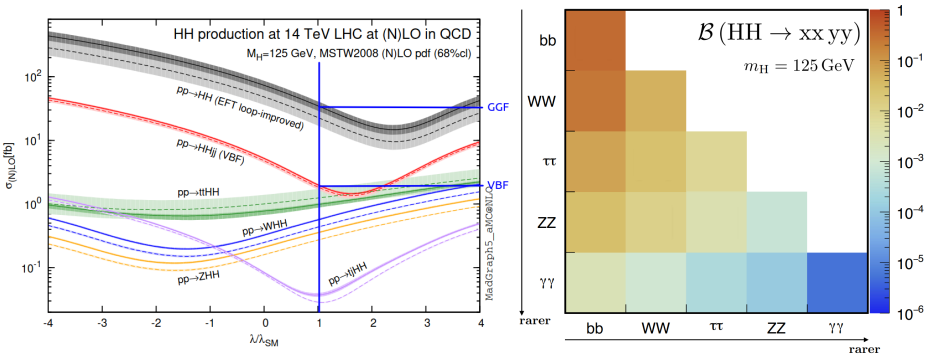


**Figure 2:** Left : HH production cross-section for the different production modes as a function of the trilinear coupling modifier. Right : HH decays channels and their branching ratios. From Ref. [3].

## 2. HH → bbbb analyses

Depending on the $p_{\mathrm{T}}$ of the Higgs boson, the two resulting jets from the decay H → bb can be well separated into two narrow cones or merged within a single large cone due to the Lorentz boost of the decay products. Each case is investigated in a resolved [5] and boosted [6] analyses. In the resolved case, the b-jet pair assignment is done through testing each combination pair using a distance measure $d = |M_{H_1} - kM_{H_2}|/\sqrt{1+k^2}$ where $k = 125/120$ is the ratio of mass peak of the leading and subleading Higgs bosons (ordered by $p_{\mathrm{T}}$). This selection is 96 % accurate for SM HH signal (fig. 3). B-jets are identified using the DeepJet CMS algorithms, together with a corrective energy regression. The event selection is split between a GGF and a VBF category, based on the presence of forward jets (cfr diagrams in fig. 1), and further refined by a boosted decision tree (BDT) trained to distinguish both processes. The VBF category is further split into two categories based on this BDT score, and the invariant mass $m_{\mathrm{HH}}$ used in the likelihood fit. The GGF category on the other hand is split into low- and high-$m_{\mathrm{HH}}$ regions, the former being more sensitive to the triangle diagram (cfr fig. 1) and therefore to $\kappa_\lambda$. A BDT score, trained to distinguish HH from backgrounds, is then used in the likelihood fit (cf. fig. 3, right). The main background contribution are QCD multi-jet events, estimated by a data-driven method using events with only 3 identified b-jets in a signal region (SR), scaled by transfer factors estimated in a control region (CR) and validated in a separate region, as illustrated on fig. 3 (middle). The resolved analysis was able to put observed (expected) upper limits on the inclusive cross-section of $\sigma_{\mathrm{HH}} < 3.9\ (7.8)\ \sigma^{SM}$ as a function of the theoretical cross-section, and for the VBF production mode of $\sigma_{VBF} < 226\ (412)\ \sigma^{SM}_{VBF}$. Constraints could also be put on the coupling modifiers $2.3\ (-5.0) < \kappa_\lambda < 9.4\ (12.0)$ and $-0.1\ (-0.4) < \kappa_{2V} < 2.2\ (2.5)$. The boosted analysis, presented in another contribution to this conference, established the following limits : $\sigma_{\mathrm{HH}} < 9.9\ (5.1)\ \sigma^{SM}_{\mathrm{HH}}$, $-9.9\ (-5.1) < \kappa_\lambda < 16.9\ (12.2)$ and $0.62\ (0.66) < \kappa_{2V} < 1.41\ (1.37)$.

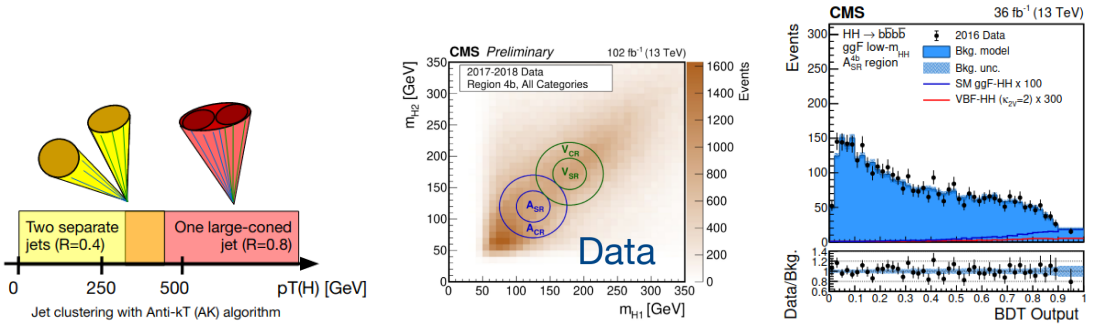


**Figure 3:** Left : Jet clustering from H $\rightarrow$ bb based on the Higgs boson $p_{\mathrm{T}}$, when the two jets are either resolved or merged. Middle : Signal region ($A_{SR}$) and control region ($A_{CR}$) in the HH 2D mass plane on both signal and data samples in the resolved bbbb analysis, together with the validation regions used for the QCD data estimation. Right : Shape of the low-$m_{\mathrm{HH}}$ region BDT score. From Ref. [5].

## 3. HH $\rightarrow$ bb$\tau\tau$ analysis

The bb$\tau\tau$ analysis [7] requires the presence of at least one hadronically decaying tau, the flavour of the other defining the event category. Several requirements are applied, notably on the number of jets and the elliptical mass requirements on H $\rightarrow$ bb and H $\rightarrow \tau\tau$ systems. Similarly to the bbbb analysis, a GGF and VBF categories are defined based on the presence of forward jets. They are further split by subcategories. For the GGF case, the categorization is based on the jet topology (boosted, resolved with one or two b-jets). The VBF categorization is based on a multiclassication deep neural network (DNN), trained at differentiating VBF from GGF, with additional background classes to allow better constraints in the fit. A final binary DNN is then used to discriminate signal from background in all categories (trained together), its score used in each category for the likelihood fit (fig. 4, right). QCD multi-jet background is estimated using an ABCD method, averaged between two reweighted CRs, as illustrated on fig. 4 (left). Other backgrounds are taken from simulation, the $t\bar{t}$ and Drell-Yan processes have their normalization constrained from CR measurements. Upper cross limits computed at $\sigma_{\mathrm{HH}} < 3.3\ (5.2)\ \sigma^{SM}_{\mathrm{HH}}$ and $\sigma_{VBF} < 124\ (154)\ \sigma^{SM}_{VBF}$, while coupling constraints are $-1.7\ (-2.9) < \kappa_\lambda < 8.7\ (9.8)$ and $-0.4\ (-0.6) < \kappa_{2V} < 2.6\ (2.8)$.

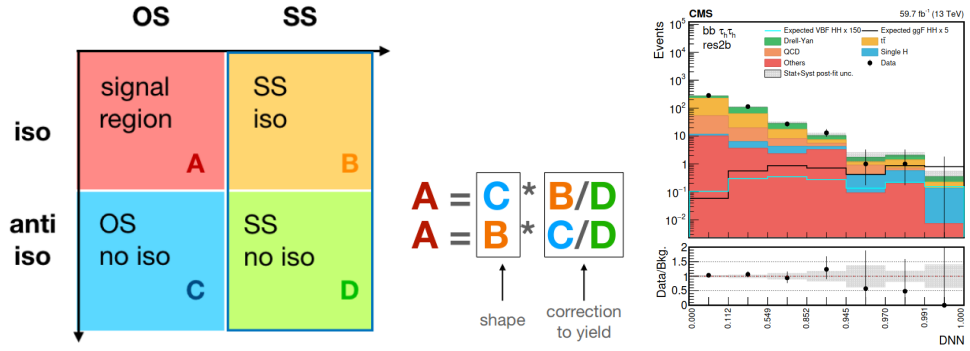


**Figure 4:** Left : ABCD regions definition for the QCD estimation. Right : DNN shape used in the likelihood fit. From Ref. [7].

## 4. HH → bb$\gamma\gamma$ analysis

In the bb$\gamma\gamma$ analysis [8] the H → $\gamma\gamma$ system has an excellent resolution (O(2 GeV)), while the resolution of the H → bb system is improved by a two-stage energy regression, on the jets separately then on $m_{\mathrm{bb}}$. A series of selection is applied to remove the main backgrounds, including photon identification, kinematic cuts and specific lepton and jet vetoes related to the top quark decay. A DNN is trained to reject the resonant ttH, and a multiclassification BDT is trained on both GGF and VBF categories to separate them and the main diphoton backgrounds. Sub-categories are defined based on its score and a HH mass estimator. The 2D decorrelated shapes of $m_{\gamma\gamma}$ and $m_{\mathrm{bb}}$ (fig. 5) are used in the likelihood fit to put upper cross-section limits of $\sigma_{\mathrm{HH}} < 7.7\ (5.2)\ \sigma_{\mathrm{HH}}^{SM}$ and $\sigma_{VBF} < 225\ (208)\ \sigma_{VBF}^{SM}$, constraints $-3.3\ (-2.5) < \kappa_\lambda < 8.5\ (8.2)$ and $-1.3\ (-0.9) < \kappa_{2V} < 3.5\ (3.1)$.

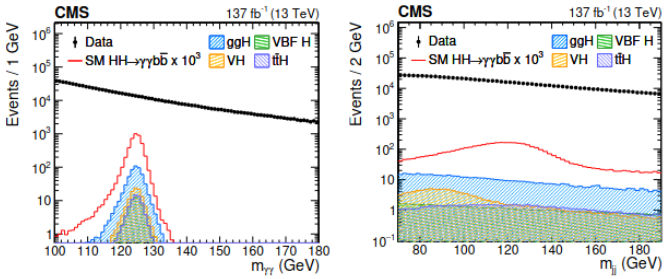


**Figure 5:** Invariant mass resolution of the two systems in HH → bb$\gamma\gamma$, comparing the HH signals from the main resonant single Higgs process and the data. From Ref. [8].

## 5. HH → bbZZ analysis

In the bbZZ analysis [9], the two Z bosons candidates are reconstructed from opposite-sign same-flavor leptons with invariant mass requirements around the Z peak mass. All irreducible backgrounds are taken from simulation, while reducible backgrounds Z + X with fake leptons are estimated by a data-driven approach from fake factors derived in CRs. A BDT is trained for each category and used in the likelihood fit (fig. 6, left). The upper inclusive cross-section is $\sigma_{\mathrm{HH}} < 32.4\ (39.6)\ \sigma_{\mathrm{HH}}^{SM}$ and constraints are set as $-8.8\ (-9.8) < \kappa_\lambda < 13.4\ (15.0)$.

## 6. HH → WWWW/WW$\tau\tau$/$\tau\tau\tau\tau$ analysis

In the "multilepton" analysis [10], seven categories are defined based on the tau flavor and W boson decays, including both leptonic and hadronic decays. A b-jet veto is applied along with several $m_{ll}$ selections depending on the category to remove some backgrounds and ensure orthogonality with the bbZZ channel. Fake leptons are estimated in the same manner as the bbZZ analysis, while electron charge flip measurement are estimated from data using a similar method. A BDT is trained for each category and used in the likelihood fit (fig. 6, right). The upper inclusive cross-section is $\sigma_{\mathrm{HH}} < 21.3\ (19.4)\ \sigma_{\mathrm{HH}}^{SM}$ and constraints are set as $-6.9\ (-6.9) < \kappa_\lambda < 11.1\ (11.7)$.

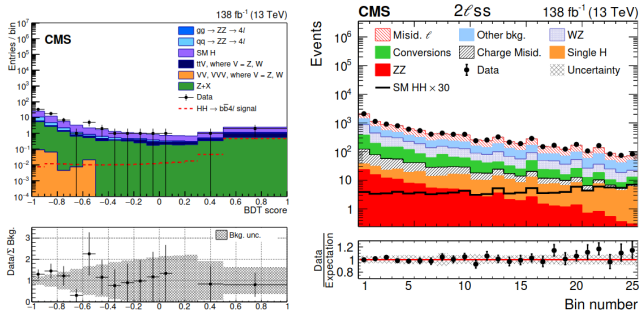


**Figure 6:** BDT score distributions in one category of the bbZZ (left) and multilepton (right) analyses. From Refs. [9, 10].

## 7. Combination

The combination of all the channels is on fig. 7, the bbbb entry combined both the resolved and boosted analyses. Compared to the 2016 combination [11] that claimed an upper limit of $\sigma_{\mathrm{HH}} < 22.2\,(12.8)\,\sigma_{\mathrm{HH}}^{SM}$, the Run-2 combination [12] achieved an upper limit of $\sigma_{\mathrm{HH}} < 3.4\,(2.5)\,\sigma_{\mathrm{HH}}^{SM}$. The combined coupling modifier constraints are $-1.24 < \kappa_\lambda < 6.49$ $(-11.8(-7.1) < \kappa_\lambda < 18.8(13.6)$ in 2016) and $0.67 < \kappa_{2V} < 1.38$, excluding for the first time a zero value of $\kappa_{2V}$ at 6.6 $\sigma$ CL.

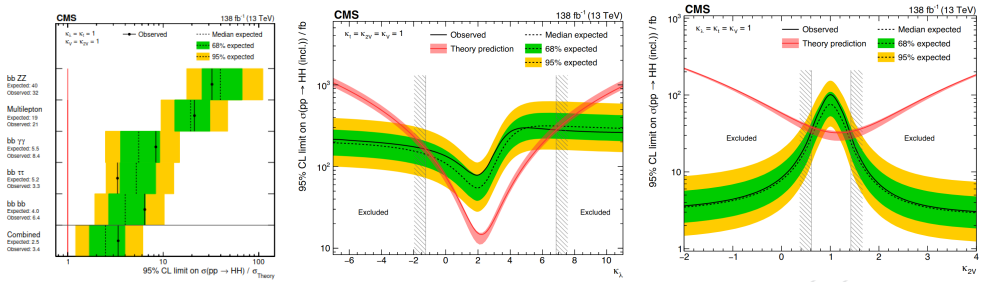


**Figure 7:** BDT score distributions in one category of the bbZZ (left) and multilepton (right) analyses. From Ref. [12].

## 8. Conclusion

In this document the different HH non-resonant searches from the CMS collaboration with public results as of July 2022 were presented as well as their combination. Limits were derived on the inclusive and VBF cross-sections, including an interpretation in the $\kappa$-framework with exclusion limits on the coupling modifiers $\kappa_\lambda$ and $\kappa_{2V}$. Additional results in terms of additional couplings, effective field theory (EFT) interpretations and resonant results were also provided by the different channels but were not the focus of this document. The Run-2 results have exceeded the expectations based solely on the luminosity increase, mostly because of better reconstruction and b-tagging techniques, additional final states are considered compared to the 2016 results, as well as a new VBF measurement focus. With that in mind, there is hope that the HEP community could reach the theoretical HH cross-section by the end of Run-3.

## References


[1] ATLAS collaboration, *Observation of a new particle in the search for the standard model higgs boson with the atlas detector at the lhc*, *Physics Letters B* **716** (2012) 1 [1207.7214].

[2] CMS collaboration, *Observation of a new boson at a mass of 125 GeV with the CMS experiment at the LHC*, *Physics Letters B* **716** (2012) 30 [1207.7235].

[3] J. Alison et al., *Higgs boson potential at colliders: Status and perspectives*, *Rev. Phys.* **5** (2020) 100045 [1910.00012].

[4] CMS collaboration, *The CMS experiment at the CERN LHC. The Compact Muon Solenoid experiment*, *JINST* **3** (2008) S08004. 361 p.

[5] CMS collaboration, *Search for Higgs Boson Pair Production in the Four b Quark Final State in Proton-Proton Collisions at s=13 TeV*, *Phys. Rev. Lett.* **129** (2022) 081802 [2202.09617].

[6] CMS collaboration, *Search for nonresonant pair production of highly energetic Higgs bosons decaying to bottom quarks*, 2205.06667.

[7] CMS collaboration, *Search for nonresonant Higgs boson pair production in final state with two bottom quarks and two tau leptons in proton-proton collisions at* $\sqrt{s} = 13$ *TeV*, 2206.09401.

[8] CMS collaboration, *Search for nonresonant Higgs boson pair production in final states with two bottom quarks and two photons in proton-proton collisions at* $\sqrt{s} = 13$ *TeV*, *JHEP* **03** (2021) 257 [2011.12373].

[9] CMS collaboration, *Search for nonresonant Higgs boson pair production in the four leptons plus two b jets final state in proton-proton collisions at* $\sqrt{s} = 13$ *TeV*, 2206.10657.

[10] CMS collaboration, *Search for Higgs boson pairs decaying to WWWW, WW*$\tau\tau$*, and* $\tau\tau\tau\tau$ *in proton-proton collisions at* $\sqrt{s} = 13$ *TeV*, 2206.10268.

[11] CMS collaboration, *Combination of searches for higgs boson pair production in proton-proton collisions at* $\sqrt{s} = 13$ TeV, *Phys. Rev. Lett.* **122** (2019) 121803.

[12] CMS collaboration, *A portrait of the higgs boson by the cms experiment ten years after the discovery*, *Nature* **607** (2022) 60.